What cooling systems can be implemented to enhance occupants' thermal comfort in highly glazed spaces?

Shengqiang Shi[1,2], Abdelatif Merabtine[3,*] , Rachid Bennacer[4]
[1] UR LASMIS, Université de Technologie de Troyes, 12 Rue Marie Curie, 10300 Troyes , France
[2] EPF Campus de Troyes, Rosière-prés-Troyes, 10430, France
[3]École de Technologie Supérieure (ÉTS), University of Québec, 1100 Rue Notre-Dame Ouest, Montreal, QC H3C 1K3, Canada
[4] LMT/ENS-Paris-Saclay/CNRS/Université Paris Saclay, Gif-sur-Yvette, 91190, France

Abstract

When integrating a radiant cooling system into highly glazed buildings, the uneven distribution of temperature and humidity caused by a long exposure to direct solar radiation becomes increasingly pronounced, thereby affecting indoor thermal comfort. Existing research has focused on analysing either radiant cooling systems or air handle unit. More importantly, the use of numerical models to analyse the impact of indoor environment and thermal comfort over the dynamic moving of sun patch is still rarely designed. Therefore, this study presents an attempt to assess of the impact of various cooling systems on both building thermal behaviour and thermal comfort within glazed spaces through experimental and simulation models. The evaluation of indoor thermal comfort involves the use of the Thermal Manikin and Givoni Diagram. The findings reveal that the presence of the sun patch has a high significant impact on the indoor environment. This makes the cooling benefit of the radiant systems limited, mainly when the floor cooling system is used. Also, it is shown that the air handle unit has a better effect and occupants' thermal comfort.

1. Introduction

As technology advances, the ongoing desire to enhance the quality of indoor thermal environments in residential and commercial spaces consistently drives engineers and architects to develop efficient and cost-effective building designs (Dogan et al., 2022). The use of cooling systems during hot and humid season has become a prominent choice for maintaining the indoor environment comfortable. Among this cooling systems, the Air handle Unit (AHU) is used for ventilation and cooling to handle sensible heat from building spaces and outdoor air intakes (Aryal et al., 2023). The radiant cooling system cools indoor air mainly through radiation heat exchange, with a less energy use to provide a thermally comfortable indoor environment (Jin et al., 2023).

Currently, there are a number of studies on the assessment of the cooling systems in hot season. (Moftakhari et al., 2023) carried out an experimental and numerical investigations to examine the cooling loads and overall heat transfer dynamics of radiant plate and all-air systems under various operating conditions. The results show that for the same air temperature set point, the peak loads for the radiant system are slightly larger than for the all-air system, regardless of the thermal comfort. (Ye et al., 2021) conducted an experimental study of the thermal performance of radiant ceiling panels with segmented concave surfaces. The results showed that the heat flux varied significantly with incoming water temperature, while changing the water flowrate had less effect. (Feng et al., 2014) performed an experimental study to investigate how the dynamic thermal behaviour of a room differs in case a radiant system or an air ventilation system is used. Experiments showed that the cooling power of the radiant system is 18-21% higher than that of the air ventilation system when internal heat gain (metabolic and equipment) is considered. However, 75-82% of the total heat gain was absorbed when a radiant system is used versus 61-63% for air ventilation system.

Besides the number of studies on the assessment of cooling systems, very few of them have considered the effect of the evolution of direct solar radiation as an external passive heat gain (Benzaama et al., 2016). Therefore, based on experiments and numerical modelling, the presented investigation attempts to consider the sun patch exposure on the floor when various cooling systems are used. The main contributions lie on: (i) the determination of the sun position in transient condition; (ii) its effect on indoor cooling usage; and (iii) its impact on the operating conditions and indoor thermal comfort of different cooling systems during summer.

*Corresponding author.
E-mail address: abdelatif.merabtine@etsmtl.ca (A. Merabtine)

2. Materials and methods

For modelling validation purpose, we have conducted a series of experimental measurements on an outdoor experimental building located at EPF engineering school in the city of Troyes, France, as shown in Fig.1(a). The outdoor experimental building is primarily composed of three side-by-side rooms, namely testing room, control room, and technical room. Their areas are 17 m^2, 10.6 m^2 and 10.6 m^2 respectively, and their roof-to-floor heights are all 2.5m. The whole experimental building consists of insulated envelope, roof cooling system (RCS), Floor cooling system (FCS), Air handler unit (AHU), control system allowing to control the environment parameters, various measurement sensors and data acquisition system. Further details on the building and cooling systems can be found in (Shi et al., 2023).

The outdoor experimental building allows, among others, the study of the effect of real sun patch projection on the floor, instead of using light spots or heating films to simulate the heat gain of the solar radiation. To do so, two windows of the same specification (i.e. 1.02 × 1.90 m) are incorporated allowing the presence of the sun patch and its area modulation. The window-to-floor ratio (WFR) is 22.78%, which meets the current French requirement recommending the WFR of new residential buildings to be higher than 16% (Glass for Europe, 2014).

Furthermore, to assess the thermal comfort and thermal sensation indoors, thermal manikin Newton® was used to accurately and reproducibly measure thermal comfort parameters for both male and female genders under transient and thermally inhomogeneous conditions. As shown in Fig.1(b), The manikin has 34 organic shaped and independently controlled heat zones. The manikin is equipped with heaters and temperature sensors to simulate metabolic heat output rates. Moreover, the thermal manikin Newton® is equipped with ambient sensors, system acquisition, and power enclosure. the embedded thermo-physiological model of the thermal manikin provides both thermal comfort and thermal sensation indicators according to the scale of (Zhang, 2003). Extended details are given in (El akili et al., 2023, 2022; Li et al., 2023; Shi et al., 2023).

(a)

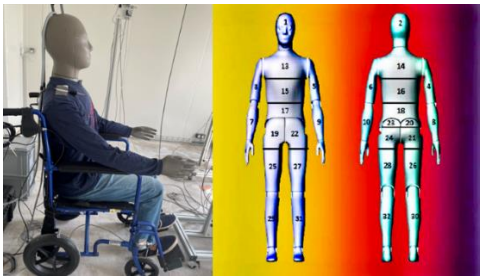

(b)

Fig.1. Experimental Building. (a) inside and outside views of the test room, control room and technical room; (b) Thermal manikin Newton®.

The considered experimental scenarios are depicted in Table 1. Before experiencing each scenario, all cooling systems were turned off and only the AHU was operating to ensure renewable air. It is worth noting here that the AHU was activated for the whole experimental period to ensure air renewal to meet the recommended air supply of 30.6 m^3/hour per person (Bellagh et al., 2021). Only in Scenario 2, the AHU cooling coil was activated. For all three scenarios, cooling systems were always turned on at 9 a.m. The setpoint was 21±0.5℃ and the cooling water temperature for the three cooling systems was maintained at 10±0.5℃. The interval time for all data collection was 10 minutes.

Table 1 Detailed information on three different experimental scenarios

	Day	Sun patch	RCS	FCS	AHU
Scenario 1	July 13-14, 2023	Yes	Yes (21℃)	No	No
Scenario 2	September 14-15, 2023	Yes	No	No	Yes (21℃)
Scenario 3	September 2-3, 2023	Yes	No	Yes (21℃)	No

3. Numerical modelling

In order to further analyse the thermal behaviour and the thermal comfort considering the effect of the sun patch, a CFD model of the test cell was developed for the above-mentioned scenarios.

3.1 Geometry

As shown in Fig.2, based on the specific dimensions of the actual test room, 1:1 direct CFD modeling was performed using COMSOL Multiphysics®. Similarly, the arrangement of the AHU, false ceilings and windows, thicknesses of the slab, ceilings, and walls, as well as the spacing between tubes, were included in the developed model. The detailed geometry of the building was kept realistic in order to discuss the real effect of the different cooling systems on the

building thermal behavior. Thus, uncertainties due to the geometrical model are reduced. Table 2 below summarizes the material properties involved in the test room.

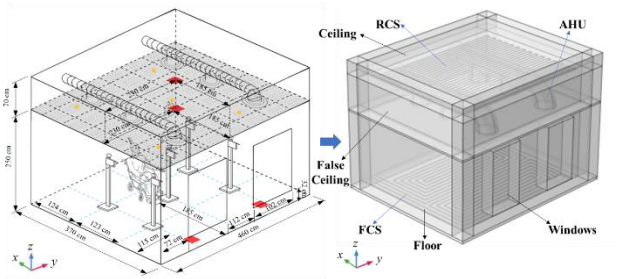

Fig.2. Physical model of the test room showing RCS, FCS and AHU

Table 2 The material properties involved in the test room.

Type of material	Dynamic viscosity (Pa·s)	Heat capacity (J/kg·K)	Density (kg/m^3)	Thermal conductivity (W/m·K)	Surface emissivity
Water	1.3×10^{-3}	4191	1000	0.57	-
Air	1.8×10^{-5}	1005	1.205	0.03	-
Silica glass	-	703	2203	1.38	0.1
Polyurethane	-	1200	413	0.06	0.92

3.2 Boundary conditions & Calculation models

Concerning the boundary conditions and model assumptions, the pressure drop of water inside the pipes of RCS and FCS was ignored for laminar fluid flow. Actually, the bottom of FCS is insulated, therefore we assumed the bottom surface adiabatic. Initial temperature input for the whole building is referenced to the initial temperature during the experiment. At the same time, in order to enable the RCS and the FCS to attenuate the space heat load while preventing condensation on the surface of the piping, the inlet water temperature was set to 10±0.5℃ during the experimental design with reference to the design guidelines (Dušan et al., 2007; DS/EN 14240:2004). Similarly, in the simulation process, the inlet temperature of each system was designed to be 10°C, respectively.

For surface-to-surface radiation, the radiative heat transfer from each surface between the false ceiling and the ceiling was ignored. The solar irradiance during the experiment is introduced by adding an interpolation function during the simulation process. Notice that due to the existence of the sun patch, localized thermal non-equilibrium occurs on the floor surface. Therefore, the indoor temperature is not solved for a homogeneous space-independent air temperature and an isothermal domain physical interface cannot be chosen.

In order to assess the indoor thermal behaviour for each cooling strategy when the sun patch occurs, four main aspects need to be considered: (i) water flow in the tubes (RCS and FCS) and air flow (AHU) are considered; (ii) heat transfer in the indoor environment mainly includes air heat convection, water heat convection, heat radiation, and heat conduction; (iii) careful consideration of radiative heat transfer between cooling surfaces and the other surfaces is required; (iv) Direct solar radiation through short wave radiation is considered. Therefore, Laminar Flow module, Heat transfer in Solids and Fluids model and Surface-to-Surface (S2S) radiation module, were used COMSOL Multiphysics®.

3.3 Grid independence & validation of the experiment

Meshing is an important step in solving finite elements. This is because by meshing it is possible to define the discretization of the computational domain into small elements, or cells, on which the equations of the physics being modelled are solved. The quality of the mesh has a significant impact on the accuracy and efficiency of the simulation, so verifying the independence of the mesh is essential in analysing finite elements. It is commonly known that the more and small the mesh grid, the more accurate solution, but will also require more computational resources and increase the simulation time. It is therefore important to strike a balance between accuracy and efficiency when choosing the mesh size.

As shown in Fig.3, at the initial stage of meshing, in order to obtain a high-quality mesh, a structured mesh is obtained by user-controlled meshing using a sweeping mode. Where Fig. 3(b) is a further refinement of the mesh based on Fig. 3(a). And Fig.3(c) is the unstructured mesh with linearly increasing density at the layer boundaries obtained by discretizing each domain using a physical field control mesh with free tetrahedral components of regular mesh size.

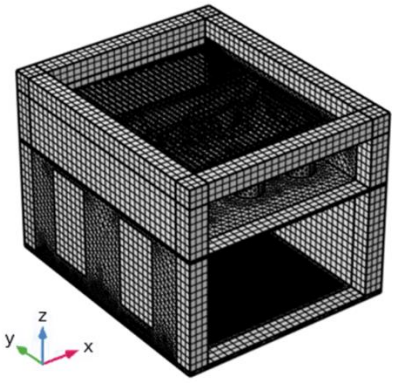

(a)

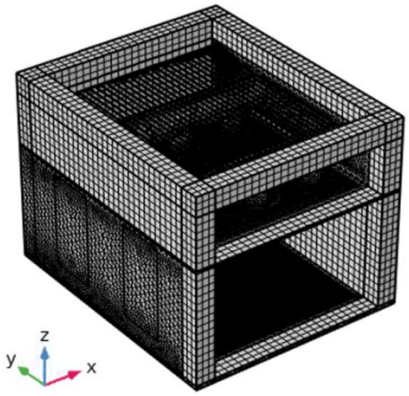

(b)

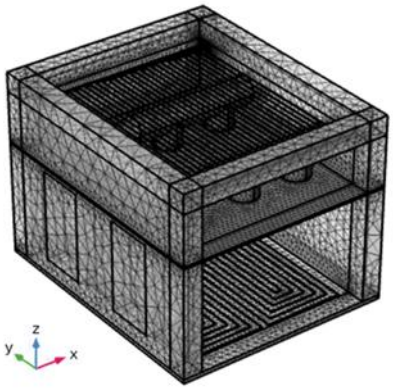

(c)

Fig.3. The existing geometric models are meshed in different ways. (a) User control grid 1; (b) User control grid 2; (c) Physical field control grid (Normal).

In order to verify the grid independence, Scenario1 was used as a case study for these three models with different grid divisions, and the optimal grid division scheme was determined by comparing the results of the calculations as well as the CPU usage time, as shown in Fig. 4. Table 3 summarizes the characteristics of each grid.

It can be seen from the Fig.4 that the model calculation results after three kinds of meshing all show the same trend as the experiment. Although when the sun patch appears, there is still a certain gap between the simulated values and the experimental values in terms of the maximum indoor temperature. However, by calculating the Coefficient of variation of RMSE (CV-RMSE), it can be found that the linear regression of the simulated value is only about 4%, which is far less than the threshold of 15% proposed by ASHRAE, 2014. Therefore, it shows that the simulation results are in good agreement with the experimental results. More importantly, by comparing the model calculation results after three different mesh divisions, it can be found that the curves presented are almost consistent, verifying that the meshes have good independence.

By comparing Table 3, it can be found that the number of grids obtained by using the two methods (b) and (c) is about 1,000,000 more grids than the method (a). However, method (c), that is using the Physical field control grid (Normal) method, obtains the model with the least CPU time, which greatly reduces the computing time.

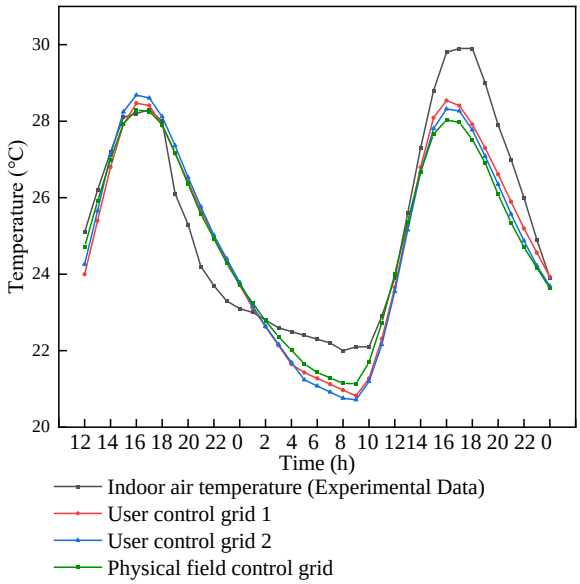

Fig.4. The influence of different refinement tests based on the indoor air temperature fluctuation.

Table 3 Three defined element sizes to investigate the validity of the mesh.

Designation	Defined element	Number of elements	Real-time simulation	CV-RMSE
(a)	User control grid 1	2,854,011	45h53min	3.7%
(b)	User control grid 2	3,372,629	44h43min	4.2%
(c)	Physical field control grid (Normal)	3,401,227	2h29min	4%

4. Results and discussion

Fig.5 shows the changes in sun patch on indoor floor surfaces as the sun moves over time during the experiment and simulation process. By comparing experiments and simulations, it can be found that the sun patches during the simulation process can better describe the actual change process, and the position and shape of the sun patches at the same time are in good agreement.

Although the temperatures at different points on the slab were measured, the temperature changes in the overall region of the sun patches could not be represented at all times, as one sensor cannot allow a surface temperature field, otherwise one may use an IR camera with recording. However, the simulation can make up for the shortcomings in a better way, and thus it is more straightforward to find out the changes of the local thermal non-equilibrium over time. It is clearly noticed that there is a substantial difference (up to 15°C) between the surface temperatures in and outside the sun patch area. But more importantly, we can numerically notice that in the overheated area, due to the slow movement of the sun patches and the high intensity of outdoor direct solar radiation, the slab is kept heated even the sun patch moves and disappears. The existence of thermal inertia prevents the heat from dissipating instantaneously, resulting in heat stacking (especially between 13:00 and 16:00), and overheating becomes more prominent.

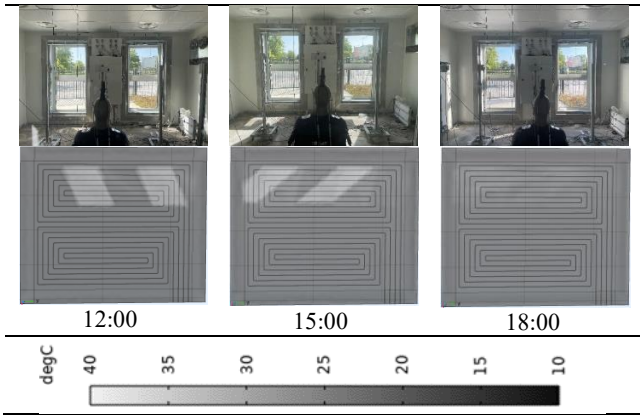

Fig.5. Comparison between experimental and numerical sun patch and visualization overt time

4.1 Scenario 1: RCS

Fig.6(a) shows the variation of indoor air temperature when RCS is used. One can find that before sun patch appears, indoor air temperature follows a consistent trend with outdoor air temperature due to the renewable air supplied by the AHU. However, when the sun patch appears, the indoor air temperature increases and overheating occurs. It can also be noticed that the outdoor maximum temperatures for both days are almost similar but the indoor temperatures for the second day are still higher than the first day. This is attributed to the fact that the direct solar radiation was increased on the second day and dominated in affecting the indoor air. Numerically, this phenomenon is not observed due to the model assumptions of the short-wave radiation module.

Fig.6(b) shows the indoor thermal comfort and thermal sensation with and without using RCS. As can be seen, without using RCS, body average thermal comfort first rises then becomes "uncomfortable" due to overheating when sun patch occurs, at this time body average thermal sensation is warm. When the sun patch disappears, the thermal comfort increases. In contrast, with the RCS cooling, Body average comfort and Body average sensation showed the same trend. However, the presence of the sun patch delayed the thermal comfort from "comfortable" to "uncomfortable", and the degree of "uncomfortable" decreased.

Another advantage of simulation is that it can make up for the inability to investigate the results of the experiment. For example, it is not possible to measure the temperature gradient from the foundation to the floor surface during the display experiment to investigate the effect of the heat from the sun patch on the floor, but the simulation analysis can just make up for the shortcomings brought by the experiment. As shown in Fig.6(c), two points, the sun patch area (x=1; y=1.5) and the shaded area (x=2; y=3), were chosen to analyze the temperature change from the foundation to the floor at 12:00. It is clear from the figure that due to the presence of the sun patch, the local temperature of the ground is increased and at the same time the temperature at a height of 4 cm down from the ground is affected and increased.

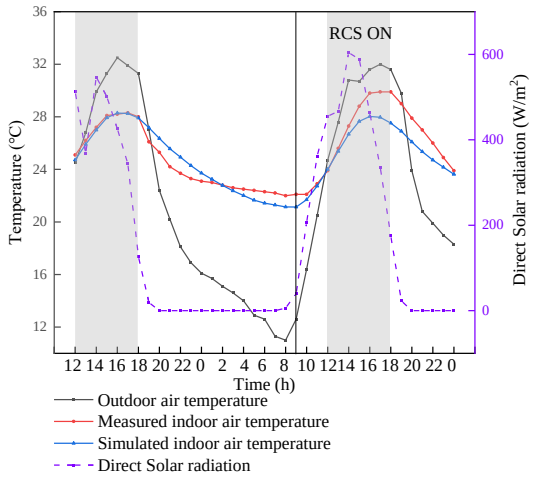

(a)

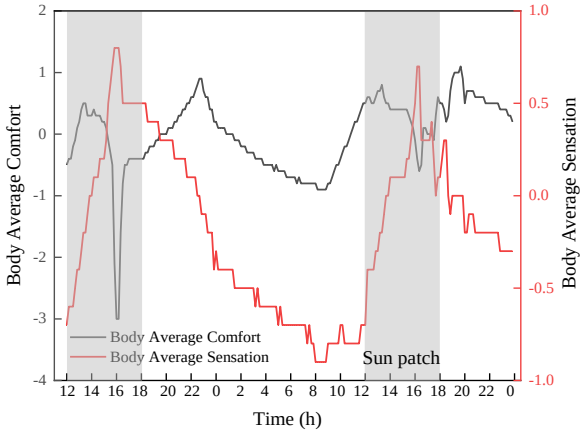

(b)

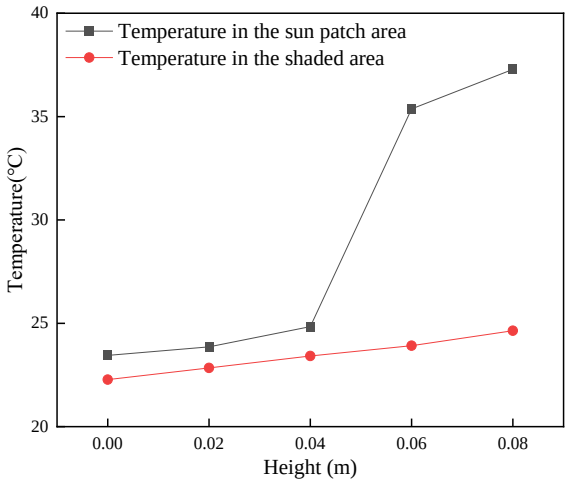

(c)

Fig.6. Impact of using RCS on the indoor environment and the thermal comfort (a) variation of indoor air temperature; (b) thermal comfort and thermal sensation; (c) is floor section temperature at different locations with or without sun patch.

4.2 Scenario 2: AHU

Fig.7(a) shows the impact of using AHU on indoor environment and thermal comfort. It can be noticed that the maximum outdoor air temperature as well as the direct solar radiation are nearly the same on both days. When the AHU is used as a cooling system, the indoor air is significantly reduced (from 32°C to 28°C). Using the Givoni diagram, it can also be seen that when the AHU is used for cooling, the indoor comfort is in the "comfortable" zone for the entire time period, even in the presence of sun patches (Fig.7(b)).

The main reason for this phenomenon is that, on the one hand, the AHU can quickly remove the sensible heat of the air in the room; on the other hand, no matter whether the RCS system or the FCS system is used, there is still a mix of fresh air from outside in the room. The presence of direct solar radiation makes the outdoor fresh air temperature too high, which inhibits the cooling effect of the radiant heat transfer system. However, when the AHU is used for cooling, the fresh air is pre-treated when it enters the room, thus controlling the temperature of the fresh air and greatly improving the cooling effect. Although the use of AHU cooling enables a comfortable indoor environment, it can be seen in Fig.7(c) that the local temperature at the ground level and the temperature in the depth of 4 cm below the ground level are still affected by the sun patch.

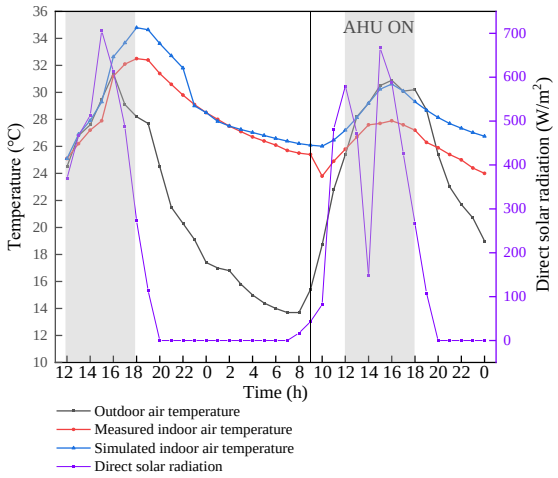

(a)

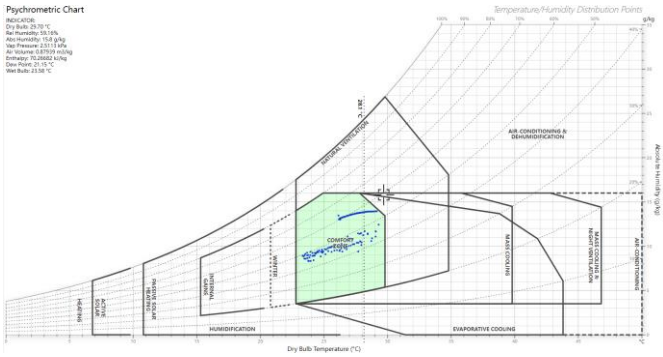

(b)

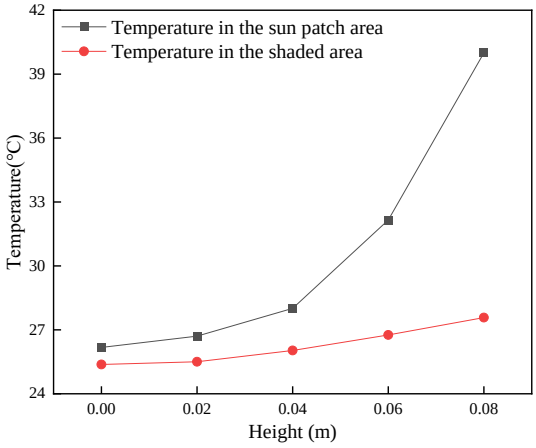

(c)

Fig.7. The impact of using AHU on indoor environment and thermal comfort in the presence of sun patch. (a) The variation of indoor air temperature with and without AHU; (b) Using Givoni diagram to analyse indoor thermal comfort when AHU is turned on; (c) is floor section temperature at different locations with or without sun patch.

4.3 Scenario 3: FCS

Fig.8(a) shows the indoor air temperature with and without FCS. In terms of indoor air temperature variations, the results are in close agreement with the RCS. With regards to the experimental and simulation results, the cooling effect of the two radiant cooling systems is not satisfactory. With the FCS is turned on, the presence of sun patches still increased the indoor temperature by 1.6°C.

Fig.8(b) shows the comparison of indoor thermal comfort and thermal sensation with and without FCS. Comparing the indoor thermal comfort with and without the FCS, it can be found that the FCS is able to attenuate the discomfort when it is turned on, but the effect is the worst among the three cooling systems. It can be seen from Fig. 8(c) that despite the use of FCS for cooling at this time, the ground temperature still rises in the presence of the sun patch, which dominates the effect at this time.

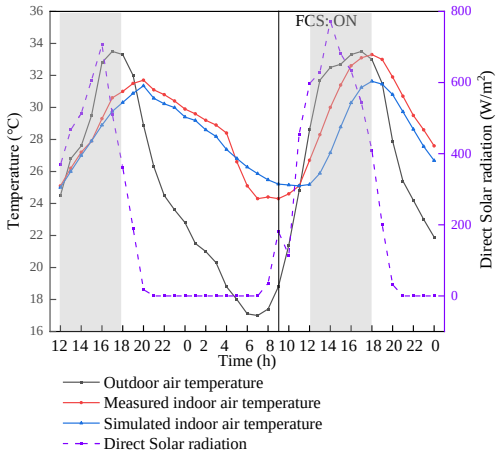

(a)

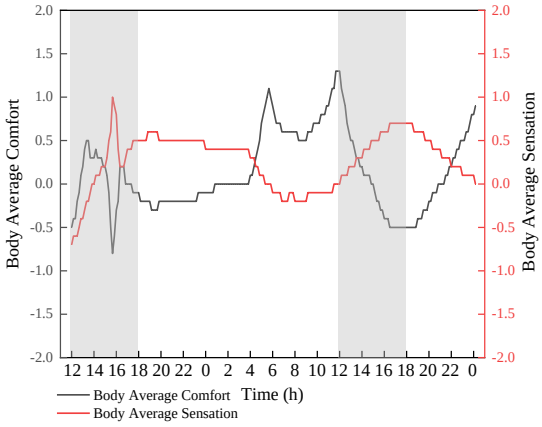

(b)

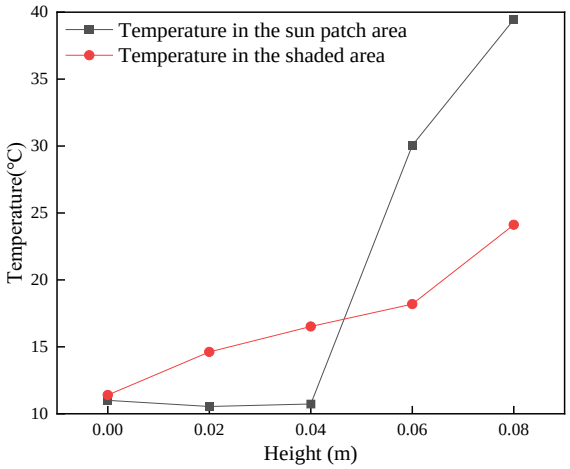

(c)

Fig.8. Impact of using FCS on the indoor environment and the thermal comfort (a) variation of indoor air temperature; (b) thermal comfort and thermal sensation; (c) is floor section temperature at different locations with or without sun patch.

5. Conclusion & Future work

This study provides an extensive evaluation of how different cooling systems affect thermal dynamics and comfort levels in highly glazed buildings using both experimental measurements and numerical simulations. Based on the climatic conditions, sun patches are numerically simulated using the external radiation source model built into the surface-to-surface radiation physics field in COMSOL Multiphysics®. The assessment of indoor thermal comfort utilizes the Thermal Manikin Newton® and Givoni Diagram. The effect of solar patches on indoor environments is significant, which causes indoor air temperatures to rise despite the presence of radiant cooling systems. The cooling effect of the radiation systems are unsatisfactory, and the floor cooling system has the worst cooling effect. Among the three different cooling systems, air handle unit has a better effect on increasing thermal comfort.

For future work, mitigation of overheating caused by sun patches on RHC systems was a subject that requires a lot of work, including novel active and passive technologies. Active cooling techniques are widely used. Ventilation strategies are the most used ones since it permits dual benefits including both overheating decreasing and indoor air quality improvement, but seem to be less efficient in summer season. Even it is less used, using full return water in closed loop combined with a control strategy is also a promising technique. Passive cooling systems including metamaterials used as radiative coolers take currently several forms including, films (polymer and inorganic material), spray, paints, etc. They can achieve a substantial cooling impact by possessing a high infrared emissivity

(within the range of 8μm-13μm), enabling it to release heat into the cold expanse of outer space through the atmospheric window. Additionally, its remarkable solar reflectivity ensures minimal absorption of solar energy. This dual feature facilitates swift and efficient cooling without energy consumption.

Acknowledgement

This work was supported by the China Scholarship Council [grant numbers 202208120025]. Authors would like to thank Le Conseil Départemenal de l'Aube and Troyes Champagne Métropole for their funding and help to carry out this study. The authors also gratefullyacknowledge the help from Yanwen Lian in guidance on schematic drawing.

References

Aryal, A., Chaiwiwatworakul, P., Chirarattananon, S., 2023. An experimental study of thermal performance of the radiant ceiling cooling in office building in Thailand. *Energy and Buildings* 283, 112849.

Dušan P., Babiak, J., Bjarne W. O., 2007. *Low temperature heating and high temperature cooling: embedded water based surface heating and cooling systems*. Rehva.

Bellagh, L., Merabtine, A., Kheiri, A., Mokraoui, S., Kauffmann, J., 2021. Studies on how to counteract overheating caused by sun patch exposure in ventilated highly glazed spaces heated by floor heating systems. *Solar Energy* 220, 991–1005.

Benzaama, M.-H., Lachi, M., Maalouf, C., Mokhtari, A.-M., Polidori, G., Makhlouf, M., 2016. Study of the effect of sun patch on the transient thermal behaviour of a heating floor in Algeria. *Energy and Buildings* 133, 257–270.

Dogan, A., Kayaci, N., Demir, H., Kemal Sevindir, M., 2022. An experimental comparison of radiant wall and ceiling cooling system integrated with ground source heat pump and direct expansion fan coil system in a highly glazed office room. *Energy and Buildings* 273, 112412.

DS/EN 14240:2004 - Ventilation for buildings - Chilled ceilings - Testing and rating.

El akili, Z., Bouzidi, Y., Merabtine, A., Polidori, G., Kauffmann, J., 2023. Thermal comfort of Frail People under dynamic and non-uniform thermal environments using a thermal manikin with thermoregulatory control: An experimental study. *Energy and Built Environment* 4, 477–491.

El akili, Z., Bouzidi, Y., Merabtine, A., Polidori, G., Kauffmann, J., 2022. Assessment of thermal comfort of frail people in a sitting posture under non-uniform conditions using a thermal manikin. *Building and Environment* 221, 109334.

Feng, J. (Dove), Bauman, F., Schiavon, S., 2014. Experimental comparison of zone cooling load between radiant and air systems. *Energy and Buildings* 84, 152–159.

Glass for Europe. https://glassforeurope.com/daylight-and-glazing-requirements-in-new-construction/.

Zhang, H., 2003. Human Thermal Sensation and Comfort in Transient and Non-Uniform Thermal Environments. Center for Environmental Design Research (CEDR), University of California, Berkeley. PhD dissertation.

Jin, W., Wang, Y., Wang, C., Jia, L., Moon, D., Song, S., 2023. A novel cooling capacity prediction model for open-type cooling radiant ceiling. *Journal of Building Engineering* 74, 106846.

Li, T., Merabtine, A., Lachi, M., Bennacer, R., Kauffmann, J., 2023. Experimental study on the effects of a moving sun patch on heating radiant slabs: The issue of occupants' thermal comfort. *Solar Energy* 255, 36–49.

Moftakhari, A., Bourne, S., Novoselac, A., 2023. All-air vs. radiant cooling systems: Analysis of design and operation factors that impact building cooling loads (ASHRAE RP 1729). *Science and Technology for the Built Environment* 29, 381–401.

Shi, S., Merabtine, A., Bennacer, R., Kauffmann, J., 2023. Experimental evaluation of the impact of real sun patch on radiant floor heating in highly glazed spaces. *Building and Environment* 244, 110799.

Ye, M., Serageldin, A.A., Radwan, A., Sato, H., Nagano, K., 2021. Thermal performance of ceiling radiant cooling panel with a segmented and concave surface: Laboratory analysis. *Applied Thermal Engineering* 196, 117280.